JTTEE5 15:372-381
DOI: 10.1361/105996306X124374
1059-9630/$19.00 © ASM International

Peer Reviewed

Microstructure and Mechanical Properties of HVOF Sprayed Nanocrystalline Cr_3C_2-25(Ni20Cr) Coating

M. Roy, A. Pauschitz, J. Bernardi, T. Koch, and F. Franek

(Submitted July 13, 2005; in revised form January 23, 2006)

The objectives of this work are to deposit nanocrystalline Cr_3C_2-25(Ni20Cr) powder by thermal spraying and to compare the performance of this coating with that obtained using conventional powder. Towards that purpose, Cr_3C_2-25 (Ni20Cr) powders with nanocrystalline grain size and with conventional grain size were deposited using OSU-SJS high-velocity oxyfuel (HVOF) system. The microstructural features, such as morphology of the coated surface, thickness of the coating, the interface of the coating with the substrate, distribution of various phases, and grain sizes etc. were characterized with the help of optical microscope, scanning electron microscope (SEM), and transmission electron microscope (TEM). The amount of oxide phases and pores were determined by means of image analyzer. The presence of various phases was identified by x-ray diffraction (XRD) technique. Hardness, elastic modulus, and indentation toughness were evaluated employing micro indentation technique. The results indicate the presence of three different zones containing only orthorhombic Cr_3C_2 phase, FCC NiCr phase, and mixture of Cr_3C_2 and NiCr phases in both coatings. The grain sizes in the nanocrystalline coating were in the range of 80 to 100 nm. Nanocrystalline coating exhibits 20% increase in hardness, 40% decrease in surface roughness, and comparable fracture toughness and elastic modulus with respect to conventional coating.

Keywords coatings for engine components, high-velocity oxyfuel (HVOF) coatings, HVOF spray parameters, nanocrystalline coatings, nanocrystalline materials, properties of coatings

1. Introduction

Cermet variety of coatings such as WC-Co and Cr_3C_2-NiCr are well known for their excellent wear behavior. Among these cermet variety of coatings, WC-Co and Cr_3C_2-NiCr coatings find application in a large variety of industrial usages (Ref 1-3). However, WC-Co coatings decarburize to W_2C, or even to elemental W on exposure to high temperature (Ref 4). Decarburization degrades the mechanical properties of the coatings. Such degradation will result in poor performances under deformation-controlled wear such as mild wear. In the regimes where wear is controlled by oxidation or by transfer layer, degradation of hardness may cause a mismatch of elastic properties at the interface between the coating and the oxide scale or the transfer layer. Such mismatch in many cases is responsible for poor wear resistance. In contrast, Cr_3C_2-NiCr coating exhibits improved performance even up to a temperature of 1173 K (Ref 5). These coatings have lower hardness and lower wear resistance than WC-Co coating. An approach to improve the hardness and hence possible wear performance of Cr_3C_2-NiCr coating is to deposit the coatings in nanocrystalline form.

Of late, several attempts have been made to deposit nanostructured coatings by thermal spraying. These attempts can be broadly divided into five categories. In the first type, which is most widely used, micron-size powders are deformed heavily by mechanical alloying to get nanoscale structure and then sprayed after agglomerating to the required size (Ref 6-11). Sometimes, nanosize powders obtained by some other means are also sprayed after agglomerating to the required sizes (Ref 12, 13). In the second approach, nanosize powders are sprayed directly (Ref 14). The third type of effort consists of spraying nano powders with gaseous precursors (Ref 15). The fourth variety is spraying the powders with liquid precursors (Ref 16). The fifth and final method of spraying coatings with nanosize grains involves designing alloys with low critical cooling rate so that on spraying they become amorphous and then heating them above their crystallization temperature to initiate devitrification (Ref 17). Because the driving force for the transformation is extremely high and the diffusion rate in the solid state at the transformation temperature is very slow, a high nucleation frequency results. As there is limited time for growth before impingement between neighboring grains, a nanoscale microstructure is formed. The present attempt of depositing nanoscale coating is somewhat similar to the fifth method. In this method nanosize grains, approximately 100 nm, in the powder particles is obtained by severe quenching.

Several investigators have reported the deposition of nanostructure cermet variety of coatings (Ref 18-26). Among these a few are on nano-structured Cr_3C_2-NiCr (Ref 24, 26). He et al. (Ref 24) deposited nanostructured Cr_3C_2-25(Ni20Cr) coating using a Sulzer Metco diamond jet system. The average particle

Manish Roy, Defence Metallurgical Research Laboratory PO, Kanchanbagh, Hyderabad, 500 058, India; **A. Pauschitz** and **F. Franek**, Austrian Centre of Competence for Tribology Viktor Kaplan-Straße 2, A 2700 Wiener Neustadt, Austria; **J. Bernardi**, University Service Centre for Transmission Electron Microscopy; and **T. Koch**, Institute of Material Science and Testing, Vienna University of Technology, A 1040 Vienna, Austria. Contact e-mail: rmanish64@rediffmail.com.

size of their coating was approximately 25 nm with a uniform microstructure and microhardness of 1020 DPH_{300}. He et al. (Ref 25) also studied the precipitation phenomena in Ni base alloy and found that the precipitation of fine Cr_2O_3 particles resulted in the retardation of grain growth. All these studies were primarily concerned with the microstructure at a nanoscale level. The macro-structural features that are important for tribological degradation are not investigated extensively for nanostructured Cr_3C_2-25(Ni20Cr) coating even though nanocrystalline Cr_3C_2-25(Ni20Cr) coating exhibited improved wear performances at ambient temperature (Ref 27) and elevated temperature (Ref 28). Further, the mechanical properties other than the hardness of these coatings are not reported. In view of this, the present work is undertaken to characterize the microstructural features and mechanical properties of the coating in a comprehensive manner and to compare it with that of conventional coating. The grain size of the coating used in this work is around 80 nm to 100 nm. This size range shows excellent stability at elevated temperature (Ref 25). As this coating is primarily for elevated temperature application, grain size of 100 nm was chosen for present investigation.

2. Experimental Details

2.1 Materials

Two types of Cr_3C_2-25(Ni20Cr) powders were used for this study. The powder with conventional grain size was supplied by Deloro Stellite GmbH (Koblenz, Germany). The powder with a nanocrystalline grains was procured from WOKA GmbH (Barchfeld, Germany). Both powders had a nominal composition of 75 wt.% Cr_3C_2 and 25 wt.% Ni-20Cr alloy. These powders were manufactured by agglomeration through spray drying followed by plasma densification. In the case of powders with a nanocrystalline grain size, an additional step of severe quenching was carried out. The micrographs of both types of powders are presented in Fig. 1. Both varieties of powders are of spherical shape. The average sizes of the powders with conventional grains and powders with nanocrystalline grains are 30 ± 10 μm. Powders with conventional grain size exhibit quite a few grains with irregular shape. Both the particles are smooth and dense. The substrate material used in this work was mild steel (MS).

2.2 Thermal Spraying

Terolab Services Austria GmbH (Vienna, Austria) carried out thermal spraying of the coating using an OSU-SJS HVOF system that originated in Duisburg, Germany. Oxygen and liquid fuel kerosene were combusted under high pressure in the chamber and the combustion product was allowed to exit into the atmosphere. The powders were fed axially into the hot stream of gases. The powders were heated in the gas stream and then deposited on the substrate at a very high speed. The spraying parameters are summarized in Table 1. The surfaces of all the specimens were grit blasted using No. 13 alumina grit and were ultrasonically cleaned in acetone prior to spraying.

2.3 Coating Characterization

2.3.1 Microstructure of the Coating. The powders and the coated surfaces were observed under scanning electron microscopy (SEM) to study the morphology. The coated samples were then sectioned using a low speed diamond saw. The sectioned surfaces were polished and examined in SEM (Philips, Model No. XL 30, Eindhoven, The Netherlands) equipped with back-scattered electron detector, energy dispersive x-ray spectrometer (EDS), and image analysis facilities. Such examination helped to determine the size and distribution of carbide particles. It also allowed the estimation of the volume fraction of oxides and pores. EDS facility was used to get further details of the composition uniformity. Various zones identified by SEM were further investigated with transmission electron microscopy (TEM) (JEOL, Model No. 200CX, Sendai, Japan) to get details about the grain sizes and the crystallinity of the phases. Electron

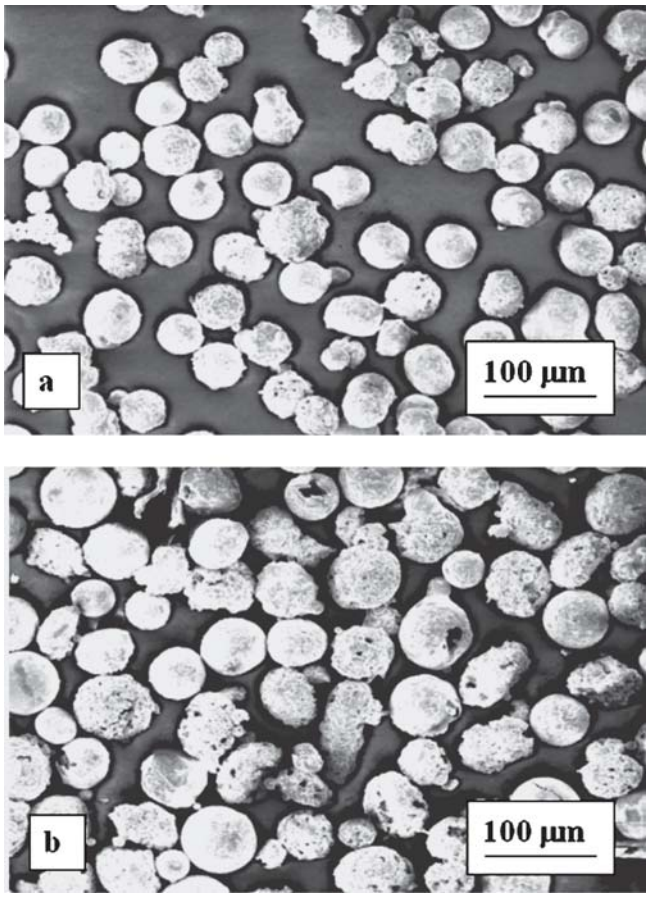

Fig. 1 The photomicrographs of the spraying powders; (a) powders with conventional grains and (b) powders with nanocrystalline grains

Table 1 The thermal spraying parameters

Parameters	Values
Liquid fuel	Kerosene
Fuel flow rate	9.3 1/h
Gas fuel	Oxygen
Fuel gas pressure	22 bar
Powder carrier gas	Air
Gas pressure	24 psi
Powder feed rate	4 kg/h
Nozzle dimension	10 × 150 mm
Spraying distance	360 mm
Power	230 V

transparent TEM samples were made by conventional grinding and subsequent thinning. Gatan (Pleasanton, CA) precision ion polishing system (PIPS) was used for this purpose.

2.3.2 X-ray Study. X-ray diffraction (XRD) patterns were obtained from the powders and the coated surfaces. The x-ray diffractometer was set at 40 KV and 30 mA with Cu-Kα radiation target and a nickel filter. The diffraction patterns were recorded at a speed of $0.01°s^{-1}$. The grain sizes of the coated samples or the powder were measured using the same diffractometer with Scherrer grain size measurement technique. XRD of the standard silica specimen was used to measure instrumental broadening and Ziegler's (Ref 29) method was used to remove instrumental broadening to get true crystal broadening of the specimen. Using the Scherrer relationship for size effect and Cauchy's correction for stress effect, the following relationship is obtained:

$$\beta Cos\theta = K\lambda/D + 4\Delta d/d \sin\theta \quad \text{(Eq 1)}$$

where β is the corrected true full width at half maximum (FWHM) of the diffraction peak, θ is the diffraction angle, K is the shape constant (close to unity), λ is the wave length of the radiation, D is the size of the crystallite, Δd is the lattice strain, and d is the lattice dimension. The parameter β cos θ was plotted against sin θ and a straight line was obtained. The intercept as per Eq 1 gives the crystal size and the slope reveals the stress.

2.3.3 Mechanical Properties of the Coatings. The microhardness of the coatings was evaluated with the help of a microhardness tester (PAAR, Model No. MHT-4, Graz, Austria). The hardness was obtained at a load of 0.2 kg for holding time of 10 s with Vickers indenter. The elastic moduli of the coatings were obtained using instrumented indentation tester equipped with a Berkovich diamond indenter at a load of 500 mN following the procedure enumerated in a separate publication (Ref 30). The elastic modulus can be calculated using equations as:

$$\frac{1}{E_r} = \frac{(1-\upsilon^2)}{E} + \frac{(1-\upsilon_i^2)}{E_i} \quad \text{(Eq 2)}$$

and E_r is given by:

$$E_r = \frac{0.89S}{\sqrt{A}} \quad \text{(Eq 3)}$$

where S is the slope of the initial part of the unloading curve and A is the contact area between the indenter and the substrate. E and E_i are the elastic moduli and ν and ν_i are the Poisson ratio of the coating and the indenter, respectively.

Finally the relative indentation toughness was estimated using Vickers indenter at a load of 1 kg. The indentation was carried out on the traverse section of the coating in the midplane region to minimize the edge and interface effects. The indenter was loaded so that one of the horizontal diagonals was parallel to the coating substrate interface. The diagonals of the indentation (a) and the cracks (l) formed at the corners of indentations were measured and used to estimate the characteristic crack length ($c = l + a$) and the indentation fracture toughness values (K_i). As most of the cracks are nearly Palmqvist type of cracks ($c/a <$ 2.5), an expression proposed by Niihara et al. (Ref 31, 32) was used. The proposed expression is:

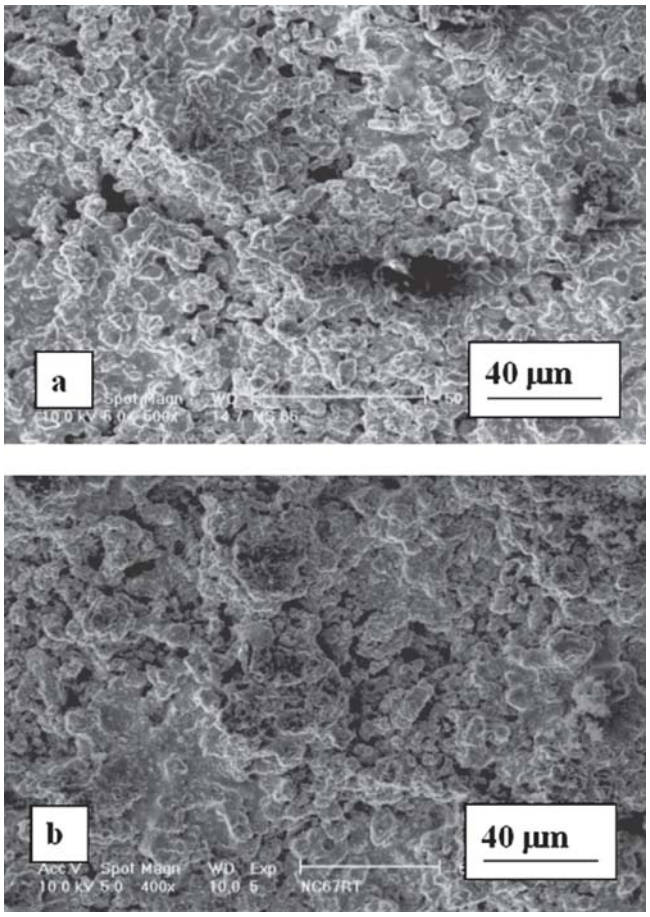

Fig. 2 SEM micrographs of the top surfaces of the coatings; (a) with nanocrystalline grains and (b) with conventional grains

$$K_i = 0.0123xE^{2/5}xH^{1/10}x(P/l)^{1/2} \quad \text{(Eq 4)}$$

where E (N/m^2) is the Young's modulus, H (N/m^2) is the hardness, and P (N) is the external load applied. A sample calculation for determination of indentation toughness is given in Appendix A.

3. Results and Discussion

3.1 Microstructure of the Coatings

The SEM micrographs from the top surfaces of both types of coatings are illustrated in Fig. 2. The surface of the coating with nanocrystalline grains (Fig. 2a) appears to be relatively smoother than that of the conventional grain. There is evidence of melting and spreading of molten powder on the surface of the coating. The extent of melting is more for coating with nanocrystalline grains than coating with conventional grain. This possibly stems from the fact that the coating with nanocrystalline grain has larger amount of high-energy grain boundary area than coating with conventional grains, assuming other related factors such as viscosity etc. are constant. As a result, for a given residence time of the particles at a given temperature, particles with higher amount of high-energy grain boundary area

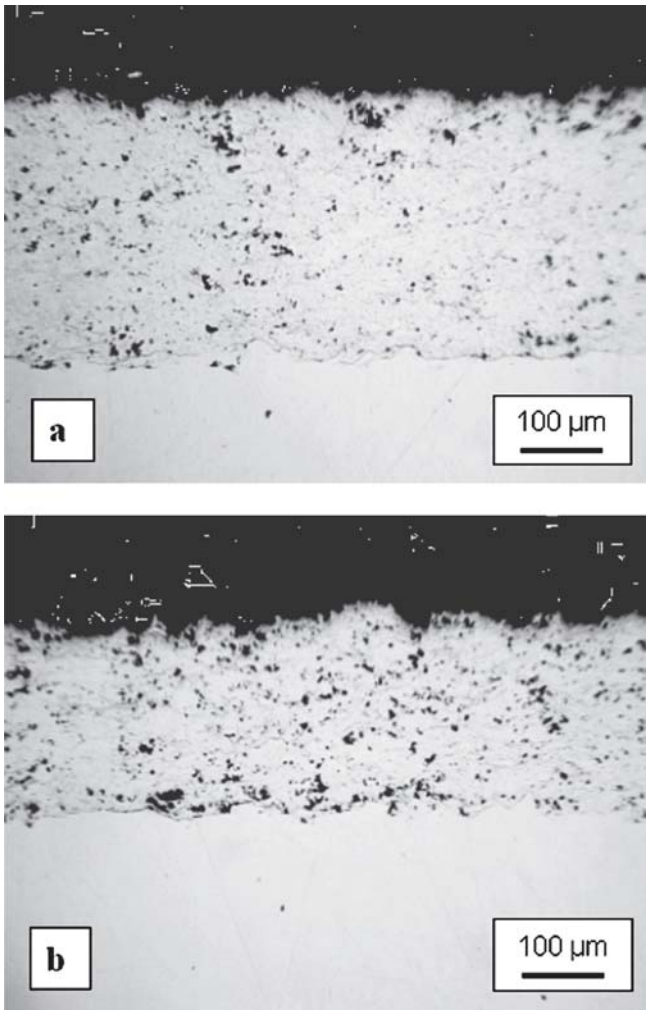

Fig. 3 Optical micrographs of the sectioned surfaces of the coatings; (a) with nanocrystalline grains and (b) with conventional grains

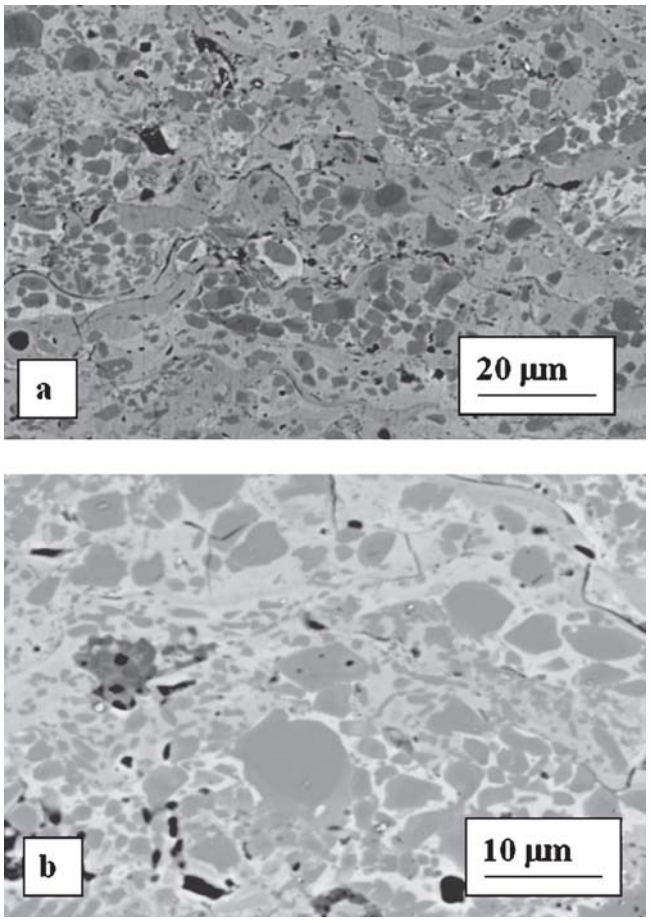

Fig. 4 High magnification back-scattered images of the transverse sections of the coatings; (a) with nanocrystalline grains and (b) with conventional grains

tend to melt more. This melting results in a decrease in roughness on the coated surface. This observation is also confirmed by surface roughness studies. Results of roughness study are given in the next section.

The optical micrographs of the sectioned surfaces of both coatings are shown in Fig. 3. Both coatings exhibit reasonably good interface with the substrate as evident from the figure. The thickness of the coating with nanocrystalline grain size is about 250 µm and that with conventional grain size is 200 µm. No cracks can be seen on the sectioned surfaces of both coatings. In both cases, coating is built by depositing lenticular splat one after the other. This type of stratified structure is common in HVOF spraying (Ref 21). In general, two types of pores can be seen. The first variety of pores is striated and can be as large as 10 µm. The second type of pores is much smaller, less than 1 µm and distributed uniformly throughout the coating. This distribution of pores is similar to that reported by Chen and Ding (Ref 33) for nanostructured zirconia coating.

The high magnification back-scattered images of the sectioned portion of the coatings are given in Fig. 4. Pores (black areas) and oxides (circular black areas) are more evident in coating with conventional grains than in coating with nanocrystalline grains. Image analysis indicates 1.5 and 2.0% porosity and 0.75 and 0.50% oxides in the coatings with nanocrystalline grains and conventional grain, respectively. Lower porosity of the coating with nanocrystalline grains stems from the fact that coating with nanocrystalline grains experience higher amount of melting and hence molten powders fill some of the pores. Similarly, a larger amount of high-energy grain boundary in the coating with nanocrystalline grain causes a higher amount of oxidation compared with conventional coating. Examination of the coated microstructure also reveals the presence of three different types of zones. The first zone appears dark. The energy dispersive spectroscopy (EDS) spectrum from the dark area is given in Fig. 5(a). This area contains primarily Cr and C indicating orthorhombic Cr_3C_2 phase. The second zone is of grey color. The EDS spectrum of this area can be seen in Fig. 5(b). This area contains all three important elements: Ni, Cr, and C. Quantitative analysis indicates this zone contains both Cr_3C_2 and NiCr. The third zone is white and the EDS spectrum (Fig. 5c) pertaining to this zone reveals NiCr as the important phase. The quantitative analysis of these zones is given in Table 2. Similar features are noted from Fig. 4(b), which corresponds to coatings with conventional grain. These results are not reproduced for the

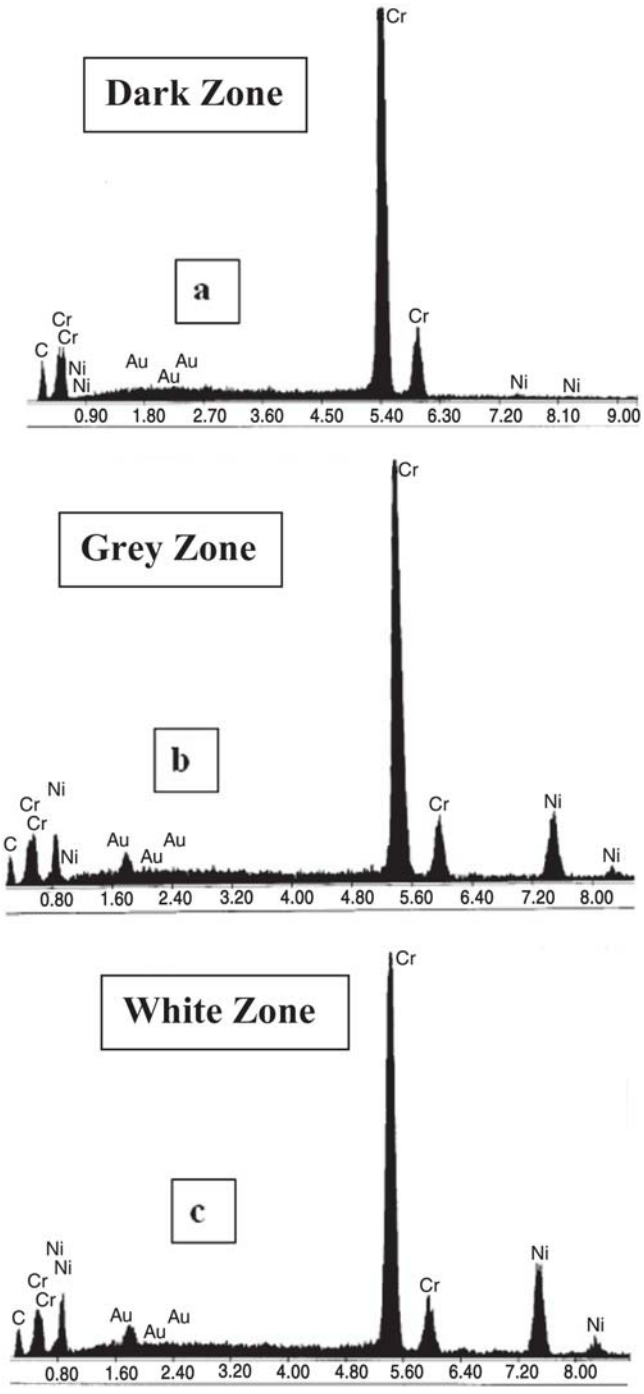

Fig. 5 The EDAX pattern of the various zones from the transverse section of the coatings; (a) dark zone, (b) grey zone, and (c) white zone

sake of brevity. Thus both coatings contain micron-size carbide phases.

The XRD pattern of the powder and coating with nanocrystalline grains is shown in Fig. 6. Most important point to be noticed is that there is no change of phases present in the powder. This is contrary to what is commonly observed for thermal sprayed WC-Co coatings (Ref 4). Interestingly, Mohanty et al. (Ref 34) observed a transformation of Cr_3C_2 phases to $Cr_{23}C_6$

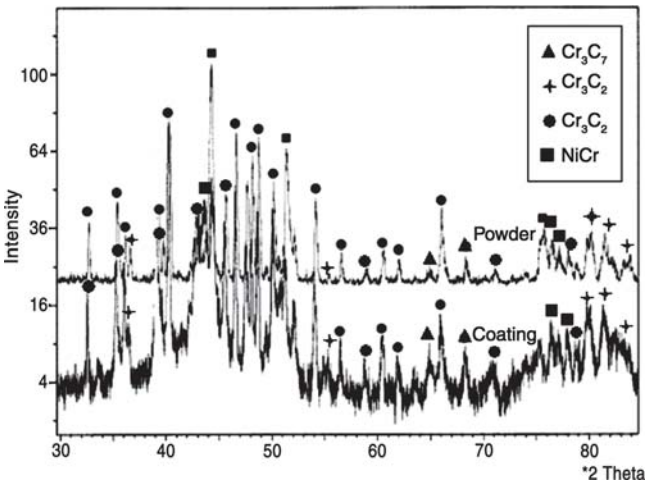

Fig. 6 The XRD pattern from the nanocrystalline powder and the coated surface.

Table 2 The composition of various elements as measured by EDAX

	Elements		
Dark zone	**C**	**Cr**	**Ni**
Wt.%	16.05	83.04	0.91
At.%	45.40	54.07	0.53
Grey zone	**C**	**Cr**	**Ni**
Wt.%	13.31	65.86	20.83
At.%	40.68	46.30	13.03
White zone	**C**	**Cr**	**Ni**
Wt.%	12.72	58.66	28.62
At.%	39.67	42.08	18.25

phases while spraying Cr_3C_2-NiCr powder with conventional grain size by Jet Kote technique. Such dissociation of Cr_3C_2 phases is not noted in the current study even in the case of nanocrystalline grains. One possible reason for this phenomenon is that the residence time of the particles in the flame is much less for the spraying system with liquid fuel. The presence of Cr_3O_2 and Cr_3C_7 can be traced in the powder and in the coated surface. There is a significant amount of amorphization of the powder as a result of spraying. X-ray study also reveals that the grain sizes of both the phases in the powder are in the range of 100 nm. Main peak of both the phases are analyzed to estimate the grain size. For NiCr phase NiCr (111) peak and for Cr_3C_2 phase Cr_3C_2 (203) peak are analyzed. However, it should be stated that this estimation is purely qualitative.

The TEM from an arbitrary zone of the coating with nanocrystalline grains is illustrated in Fig. 7 along with the electron diffraction pattern and EDS spectrum. The indexed diffraction pattern is also incorporated in Fig. 7. Very fine grain size is evident. The grain size is approximately 80 nm. The selected area diffraction (SAD) pattern also suggests fine grains. The EDS spectrum and the indexed diffraction pattern confirm the fact that the micrograph belongs to the dark zone containing Cr_3C_2 phase. There is some tendency for amorphization as can be noted from the SAD pattern. This is consistent with the observation from a XRD pattern. The bright field transmission

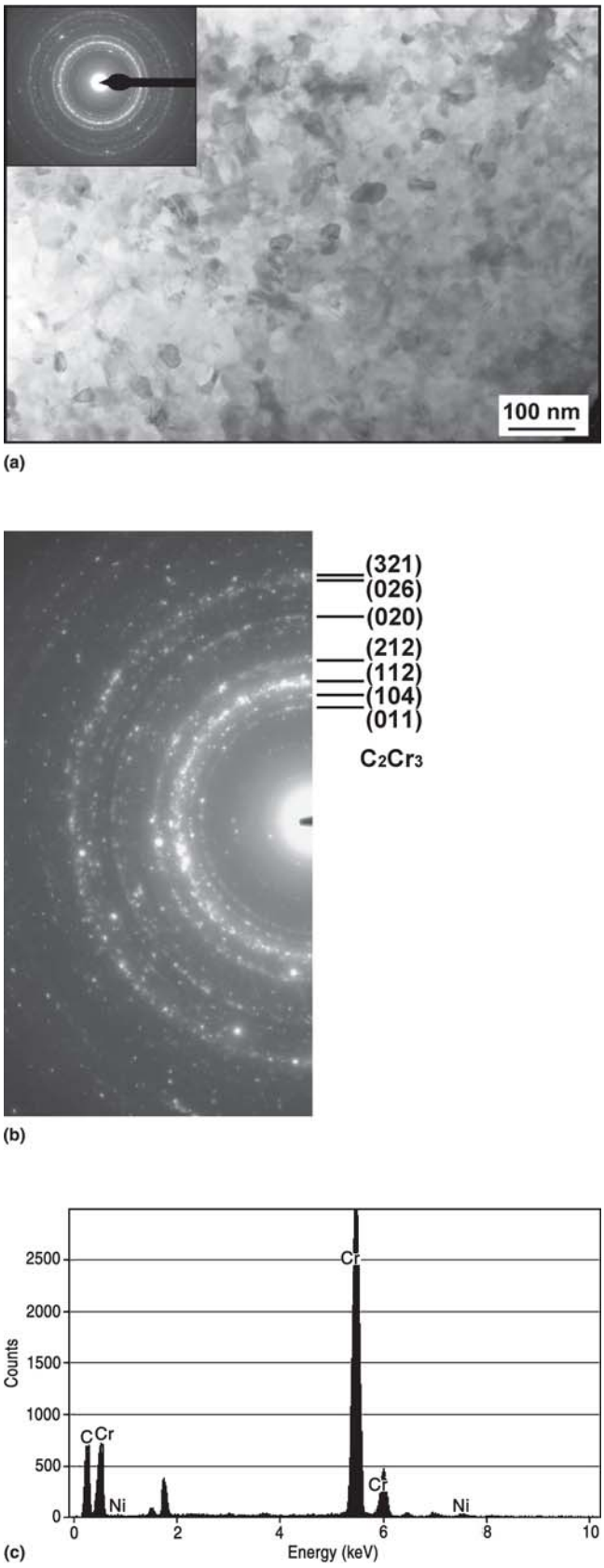

Fig. 7 The dark field TEM micrograph of the dark zone of the coating with nanocrystalline grains and the corresponding SAD pattern

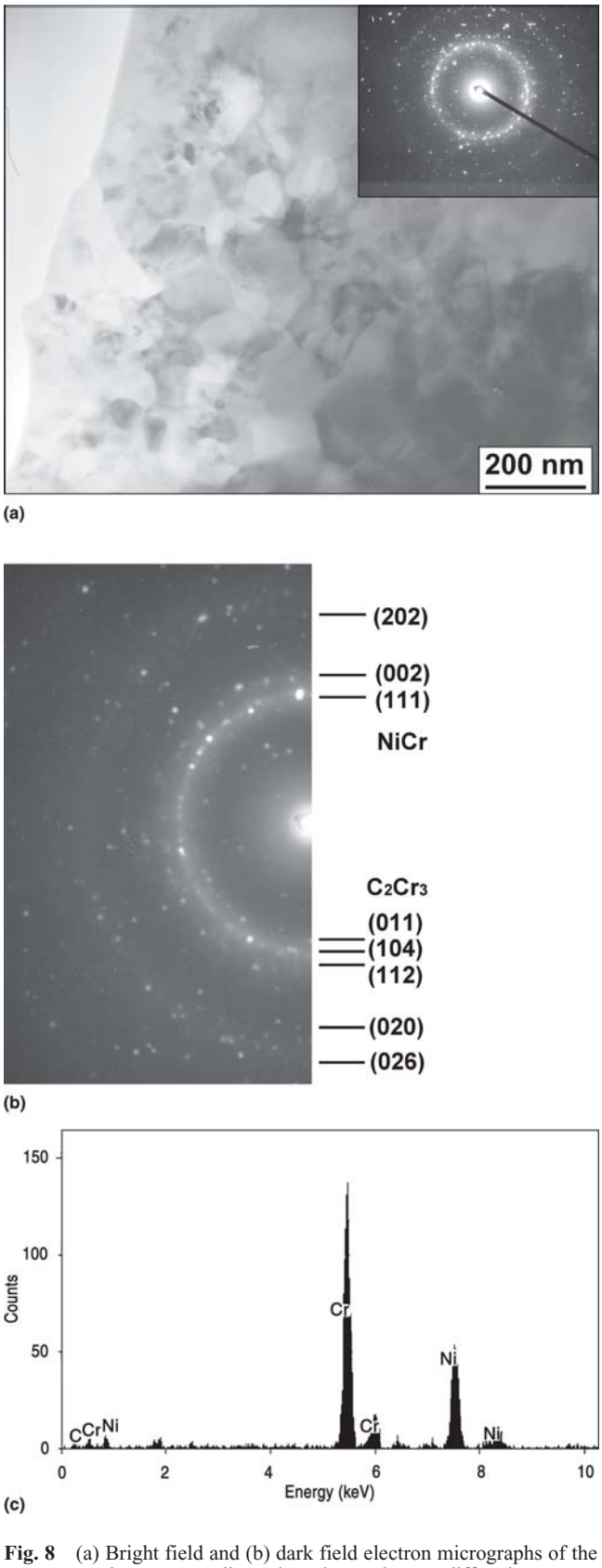

Fig. 8 (a) Bright field and (b) dark field electron micrographs of the grey zone. The corresponding selected area electron diffraction pattern confirms a mixture of nanocrystalline FCC NiCr grains and orthorhombic Cr_3C_2 grains.

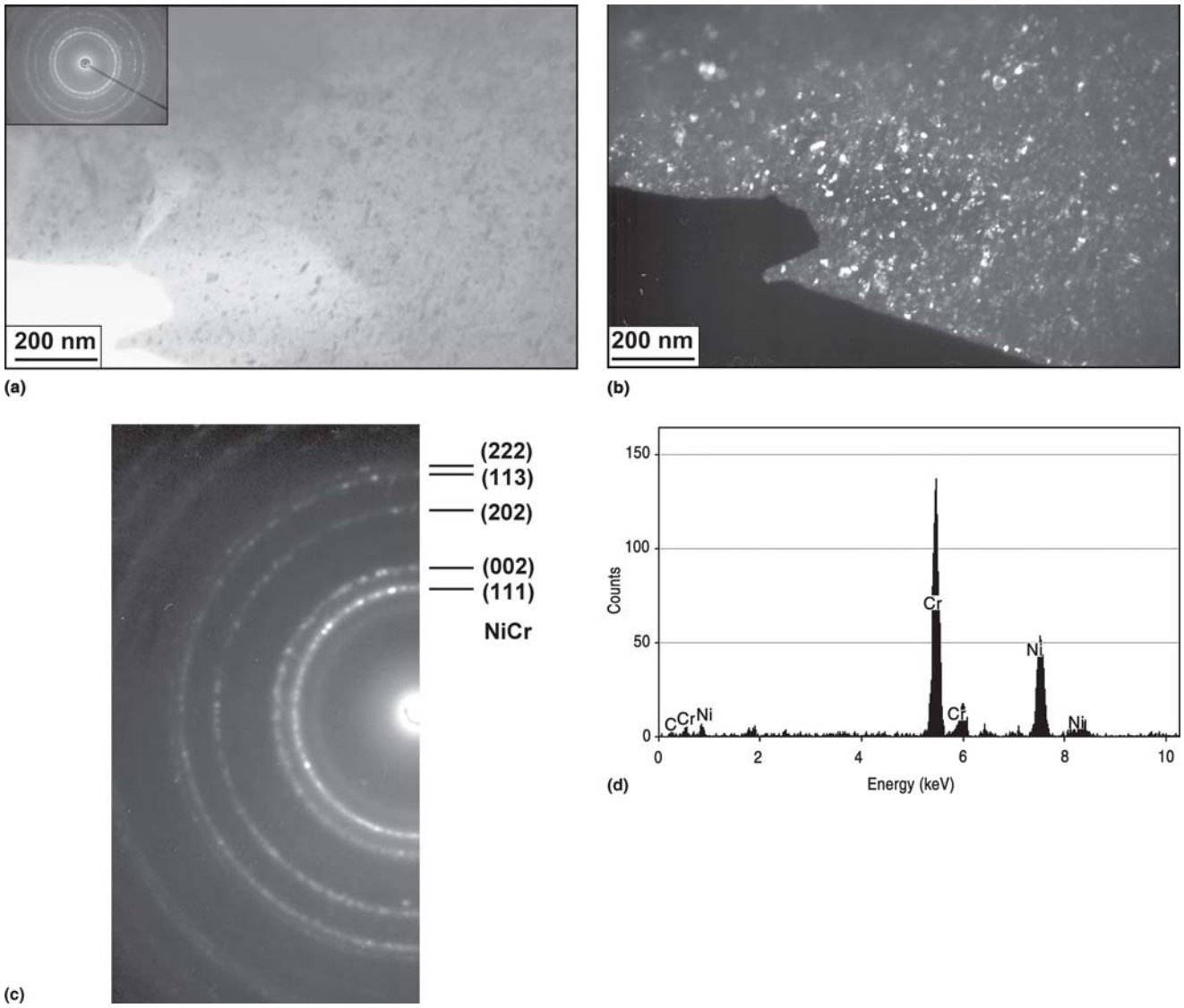

Fig. 9 TEM bright field micrograph and corresponding electron diffraction pattern and x-ray spectrum of the area containing NiCr grains showing grains with a typical diameter of about 100 nm

electron micrographs along with electron diffraction pattern and EDS spectrum from another area is presented in Fig. 8. Figure 8 also gives the indexed diffraction pattern. The indexed electron diffraction pattern and EDS spectrum confirm a mixture of nanocrystalline FCC NiCr and orthorhombic Cr_3C_2 phases. Representative TEM bright field and dark field images, corresponding electron diffraction pattern and EDS spectrum of another area are given in Fig. 9. Indexed diffraction pattern is enclosed in Fig. 9. The grains in this area are very fine, about 25 nm of size. The crystallinity of the area is evident. Based on Fig. 9, it can be concluded that the area contains primarily FCC. NiCr structure. This observation is consistent with that noted by He et al. (Ref 24), who found crystalline matrix of NiCr for Cr_3C_2-NiCr coating. In contrast, Guilemany and Calero (Ref 35) observed amorphous matrix phase in HVOF sprayed conventional Cr_3C_2-NiCr coating. There are certain areas in the grey zone, which shows presence of an amorphous zone along with nanocrystalline region. This region is possibly the one that was melted during spraying. A rapid solidification is responsible for this amorphization. A typical TEM micrograph of this region is shown in Fig. 10. A transition zone separates the purely amorphous area from an area containing a mixture of small crystals and remaining amorphous phase. Thus the coating obtained in the present work contains three different zones containing a different proportion of orthorhombic Cr_3C_2 and FCC NiCr phases. Each phase in all the three zones is having nanocrystalline grains. It is to be noted here that there is no milling involved in the present investigation. As a result there will be no strain energy, which will act as a driving force for grain coarsening. This driving force in the form of strain energy obtained during milling is particularly relevant for tribological application as the specimen undergoes deformation to a very high strain.

The TEM study of the coating with conventional grains does not reveal any additional information and hence are not repro-

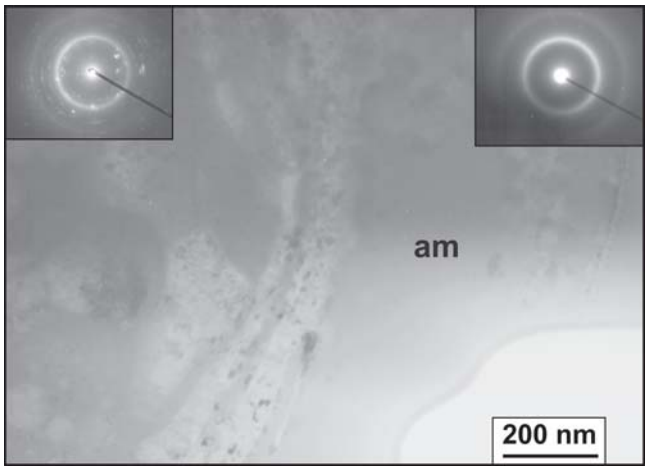

Fig. 10 Bright field electron micrograph showing a transition zone between the amorphous matrix (am) and a mixture of small grains and amorphous phase. The electron diffraction pattern comes from the area at the left side of the transition zone.

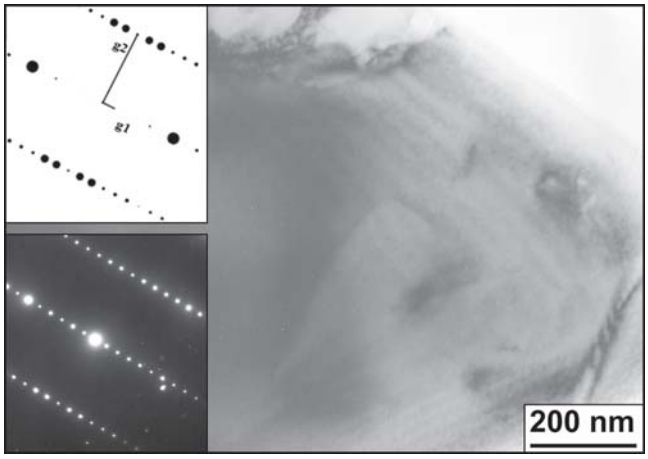

Fig. 11 TEM bright field micrograph of the Cr_3C_2 phase from coating with conventional grains with corresponding electron diffraction pattern of the orthorhombic Cr_3C_2 phase with [120] orientation

Table 3 The mechanical properties of the coating

Serial No.	Properties	Units	Coatings with nanocrystalline grain	Coatings with conventional grain
1	Roughness	μm	4.72 ± 0.22	6.43 ± 0.45
2	Elastic modulus	GPa	193 ± 19	195.5 ± 22
3	Hardness	MPa	11,400 ± 65	9786.6 ± 100
4	Indentation toughness	$MPa \cdot m^{-1/2}$	2.75 ± 0.50	2.73 ± 0.50

duced. However, the dark zone with Cr_3C_2 possesses very large grains. The typical microstructure of such a grain and the corresponding electron diffraction pattern are shown in Fig. 11. The close distance between the diffraction spots in one direction results from the (001) lattice planes of Cr_3C_2 with a lattice spacing of 1.147 nm.

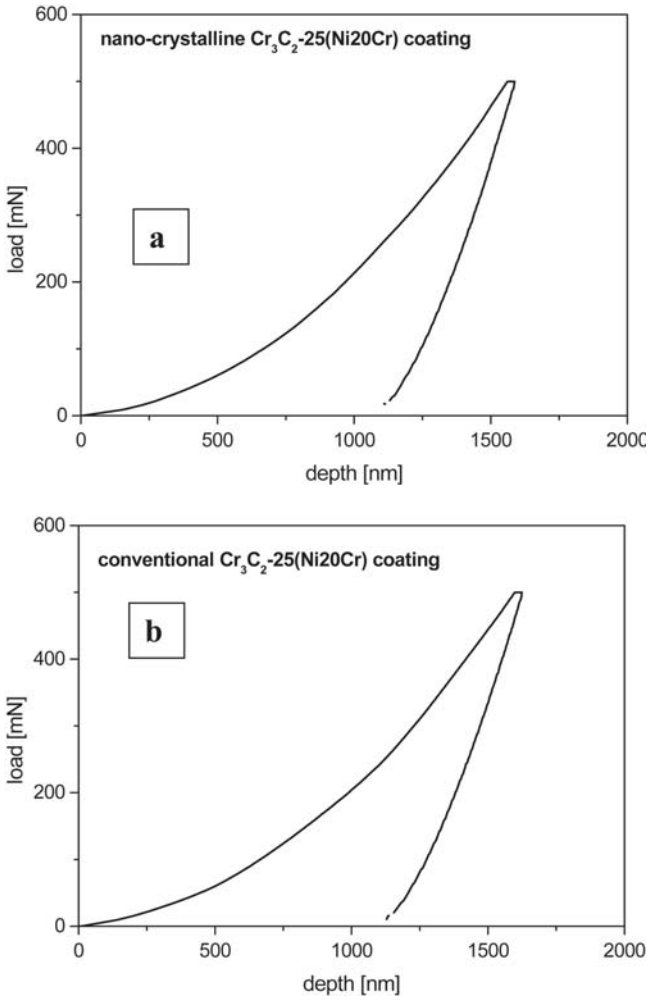

Fig. 12 The load versus displacement curve of the indentation for the coating with (a) nanocrystalline grains and (b) conventional grains

3.2 Mechanical Properties of the Coating

The various mechanical properties of the coatings with nanocrystalline grains and conventional grains are summarized in Table 3. As expected, the hardness of nanocrystalline coating is about 20% higher than the hardness of conventional coating. This value of hardness is consistent with that reported by He et al. (Ref 24) for nanostructured coating. This hardness value is also slightly higher than that reported by several investigators for conventional Cr_3C_2-NiCr coating. It is to be mentioned that the presence of Cr_2O_3 is traced in the coated layer as evident from Fig. 6. Presence of Cr_2O_3 can influence the hardness value. Perusal of the literature indicates that the hardness of Cr_2O_3 is 1200 kg/m^2 (HV2.5) (Ref 36) and that of Cr_7C_3 and Cr_3C_2 are 1600 and 1300 kg/m^2, respectively (Ref 37). These hardness values are comparable and hence the presence of the oxide phase in Cr_3C_2 is unlikely to change the overall hardness of the coating significantly. The surface roughness characterized by R_a is approximately 40% lower for nanocrystalline coating than conventional coating. The load versus displacement curves under instrumented indentation for coating with nanocrystalline grains and for coating with conventional grains are presented in Fig. 12.

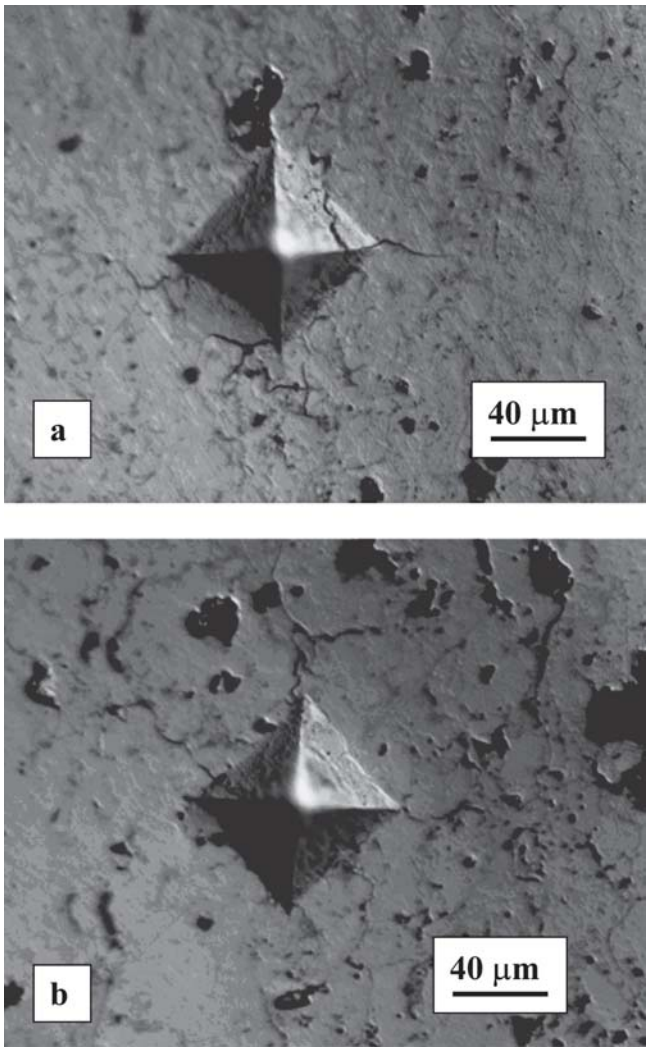

Fig. 13 Optical micrographs showing the crack around the indentation; (a) coating with nanocrystalline grains and (b) coating with conventional grains

For coating with nanocrystalline grains at a maximum load of 500 mN, the maximum depth of indentation is 1.59 μm and residual depth of indentation after final unloading is 1.11 μm. Similarly, for coating with conventional grains, the depth of indentation at a maximum load of 500 mN is 1.62 μm and the residual depth of indentation after unloading is 1.12 μm. The elastic modulus is measured as an average of ten indentation of each coating using Eq 2 and 3. The load versus displacement curves shown in Fig. 12 are essentially the ones closest to the average values. The elastic moduli of the coatings are listed in Table 3. Elastic moduli of both the coatings are comparable. Relative fracture toughness measured by the indentation method is marginally higher for coating with nanocrystalline grains as compared with coating with conventional grain. The cracks around the indentation pattern are shown in Fig. 13 for coating with nanocrystalline grains and coating with conventional grains. Apparently there is less cracking on coating with nanocrystalline grains than coating with conventional grains. It is to be noted that cracks due to indentation usually appear in the direction parallel to the coating surface along the intersplat adhesion. The bulk cermet cracks are normally found in the direction of extended diagonals of the indentation (Ref 38). Hence, the indentation toughness is expected to show different toughness behavior on different orientation. Indentation toughness of 2.7 MPa $m^{1/2}$ of Cr_3C_2-25(Ni20Cr) coating is significantly higher than that of WC-12% Co coating (Ref 39), the indentation toughness of which is 1.6 MPa $m^{1/2}$. This indentation toughness of Cr_3C_2-25(Ni20Cr) coating is also lower than the indentation toughness of plasma sprayed Al_2O_3 coating. The indentation toughness of plasma sprayed Al_2O_3 coating is about 4.5 MPa $m^{1/2}$ (Ref 40). This comparison is merely qualitative because the porosities, hardness, and the applied loads of these coatings were not equal. It should be stated that through thickness quantitative analysis of fracture toughness could not be applied in the case of indentation toughness measurement of Al_2O_3, as the applied load was very high. It is also important to note that sometimes unrealistically high fracture toughness is obtained due to indentation stress relief through extension of splat boundary and microcrack in the coatings. These microcracks dissipate energy, which otherwise drive large crack extension.

4. Conclusions

This work indicates that, using thermal spraying, it is possible to deposit nanocrystalline Cr_3C_2-25(Ni20Cr) coating having two different phases namely orthorhombic Cr_2C_3 phase and FCC Ni20Cr phase. The grain size in orthorhombic phase is between 80 to 100 nm, whereas the grain size in bcc phase is about 25 nm. The hardness of this coating is 20% higher than the hardness of the coating with conventional grains having similar composition.

Acknowledgments

The authors are grateful to FWF (Austrian Science Fund) for supporting the work through their project No M 592 and the Hochschuljubiläumsstiftung der Stadt Wien, project H-175/2002. The authors also acknowledge the support extended by WOKA GmbH, Germany, for providing the nanocrystalline powder and The Austrian Tribology Society for supporting this work.

Appendix A

Sample Calculation for Indentation Toughness

Applied load = 1 Kg = 9.8 N
Hardness = 11,400 MPa = $11,400 \times 10^6$ Pa = $11,400 \times 10^6$ N/m^2
Elastic modulus = 193 GPa = 193×10^9 Pa = 193×10^9 N/m^2
Crack size = 21.5 μm = 21.5×10^{-6} μm
Hence the equation = $0.0123E^{2/3}H^{1/10}[(P/l)]^{1/2}$
$= 0.0123(193 \times 10^9)^{1/2}(11,400 \times 10^6)^{1/10}$
$[(9.8/21.5 \times 10^{-6})]^{1/2}$
$= 0.0123 \times 32,675.6 \times 10.13 \times 675.1$
$= 401.9 \times 10.13 \times 675.1$
$= 4071.2 \times 675.1$
$= 2,748,629.8 = 2.75 \times 10^6$ N/m^2-$m^{1/2}$
$= 2.75$ MPa $m^{1/2}$

References

1. G.Y. Lai, Evaluation of Sprayed Chromium Carbide Coatings for Gas Cooled Reactor Application, *Thin Solid Films,* 1978, **53,** p 343-351
2. C.C. Li, Characterisation of Thermally Sprayed Coatings for High Temperature Wear Protection Application, *Thin Solid Films,* 1980, **73,** p 59-77
3. T.A. Taylor, M.P. Overs, J.M. Quets, and R.C. Tucker Jr., Development of Several New Nickel Alluminide and Chromium Carbide Coatings for Use in High Temperature Nuclear Reactors, *Thin Solid Films,* 1983, **107,** p 427-435
4. L. Russo and M. Dorfmann, Structure Evaluation of HVOF Sprayed NiCr-Cr3C2 Coatings, *Thermal Spraying: Current Status and Future Trends*, A. Ohmori, Ed., High Temperature Society of Japan, 1995, p 681-686
5. J. Mateos, J.M. Cuetos, R. Vijande, and E. Fernandez, Tribological Properties of Plasma Sprayed and Laser melted Cr_3C_2/NiCr Coatings, *Tribol. Intl.,* 2001, **34,** p 345-351
6. T. Grosdidier, H.L. Liao, and A. Tidu, Thermal Spray Surface Engineering via Applied Research, *Proc. 1st Int. Thermal. Spray. Conf.,* May 8-11, 2000 (Montreal, Canada), ASM Thermal Spray Society, p 1341-1344
7. M.L. Lau, E. Strock, A. Fabel, C.J. Lavernia, and E.J. Lavernia, Synthesis and Characterisation of Nanocrystalline Co-Cr Coatings by Plasma Spraying, *Nanostruct. Mater.,* 1998, **10,** p 723-780
8. M.L. Lau, H.G. Jiang, and E.J. Lavernia, Thermal Stability of Nanocrystalline Inconel 718 and Ni Prepared by High Velocity Oxygen Fuel (HVOF) Thermal Spraying, *Proc. of Intl. Thermal Spray Conf.,* C. Coddet, Ed., May 25-29, 1998 (Nice, France), p 379
9. M.L. Lau, V.V. Gupta, and E.J. Lavernia, Particle Behaviour of Nanocrystalline 316 Stainless Steel during High Velocity Oxy Fuel Thermal Spraying. *Nanostruct. Mater.,* 1999, **12,** p 319-322
10. B.H. Kear and G. Skadan, Thermal Spray Processing of Nanoscale Materials. *Nanostruct. Mater.,* 1997, **8,** p 765-769
11. H.G. Jiang, M.L. Lau, and E.J. Lavernia, Grain Growth Behaviour of Nanocrystalline Inconel 718 and Ni Powders and Coatings. *Nanostruct. Mater.,* 1998, **10,** p 169-178
12. E.H. Jordan, M. Gell, Y.H. Sohn, D. Goberman, L. Shaw, S. Jiang, M. Wang, T.D. Xiao, Y. Wang, and P. Strutt, Fabrication and Evaluation of Plasma Sprayed Nanostructured Alumina—Titania Coatings with Superior Properties, *Mater Sci. Eng.,* 2001, **A301,** p 80-89
13. T.C. Zhu, K. Yukimura, C.X. Ding, and P.Y. Zhang, Tribological Properties of Nanostructured and Conventional WC-Co Coatings Deposited by Plasma Spraying, *Thin Solid Films,* 2001, **388,** p 277-282
14. Y.C. Zhu and C.X. Ding, Plasma Spraying of porous Nanostructured TiO_2 Films. *Nanostruct. Mater.,* 1999, **11,** p 319-323
15. N.P. Rao, H.J. Lee, M. Kelkar, D.J. Hansen, J.V.R. Heberlain, P.H. McMurry, and S.L. Girshik, Nanostructure Materials Production by Hypersonic Plasma Particle Deposition. *Nanostruct. Mater.,* 1997, **9,** p 129-132
16. J. Karthikeyan, C.C. Berndt, J. Tikkanen, J.Y. Wang, A.H. King, and H. Herman, Preparation of Nanostructure Materials by Thermal Spray Processing of Liquid Precursors. *Nanostruct. Mater.,* 1997, **9,** p 137-140
17. D.J. Branagan, W.D. Swank, D.C. Haggard, and J.R. Fincke, Wear Resistant Amorphous and Nano Composite Steel Coatings, *Metal, Mater. Trans,* 2001, **32A,** p 2615-2621
18. L.L. Shaw, D. Goberman, R. Ren, M. Gill, S. Jiang, Y. Wang, T.D. Xiao, and P.R. Stutt, The Dependency of Microstructure and Properties of Nanostructured Coatings on Plasma Spray Conditions, *Surf. Coat. Technol.,* 2000, **130,** p 1-8
19. D.A. Stewart, P.H. Shipway, and D.G. McCartney, Abrasive Wear Behaviour of Conventional and Nanocomposite HVOF Sprayed WC-Co Coatings, *Wear,* 1999, **225-229,** p 789-798
20. J. He, M. Ice, S. Dallek, and E.J. Lavernia, Synthesis of Nanostructured WC-12 Pct Co Coating Using Mechanical Milling and High Velocity Oxygen Fuel Thermal Spraying. *Metal Mater. Trans.,* 2000, **31A,** p 541-553
21. B.H. Kear, R.K. Sadangi, M. Jain, R. Yao, Z. Kalman, G. Skandan, and W.E. Mayo, Thermal Sprayed Nanostructured WC/Co Hard Coatings, *J. Therm. Spray Tech.,* 2000, **9,** p 399-406
22. Y.C. Zhu, M. Huang, J. Huang, and C.X. Ding, Vacuum Plasma Sprayed Nano Structured Titanium Oxide Films, *J. Therm. Spray. Technol.,* 1999, **8,** p 219-222
23. V.L. Tellkamp, M.L. Lau, A. Fabel, and E.J. Lavernia, Thermal Spraying of Nanocrystalline Inconel 718. *Nanostruct. Mater.,* 1997, **9,** p 489-492
24. J. He, M. Ice, and E.J. Lavernia, Synthesis of Nanostructured Cr_3C_2-25(Ni-20Cr) Coatings. *Metal Mater. Trans.,* 2000, **31A,** p 555-564
25. J. He and E.J. Lavernia, Precipitation of NanostructuredCr_3C_2-NiCr Coatings, *Mater. Sci. Eng.,* 2001, **A301,** p 69-79
26. B.H. Kear, Z. Kalman, R.K. Sadangi, G. Skandan, J. Colaizzi and W.E. Mayo, Plasma Sprayed Nanostructured Al2O3/TiO2 Powders and Coatings. *J. Therm. Spray. Technol.,* **9** (200) 483-487
27. A. Manish Roy, Pauschitz, J. Wernisch, and F. Franek, The Influence of Temperature on the Wear of Cr_3C_2-25(Ni-20Cr) Coating—Comparison Between Nanocrystalline Grains and Conventional Grains, *Wear,* 2004, **257,** p 799-811
28. A. Manish Roy, Pauschitz, J. Wernisch, and F. Franek, Comparative Evaluation of Ambient Temperature Friction Behaviour of Thermal Sprayed Cr_3C_2-25(NiCr) Coatings with Conventional and Nanocrystalline Grains, *Tribol. Intl.,* 2005, **39,** p 29-38
29. T. Ekstron, C. Chatfield, W. Wruss, and M.M. Schreiber, The Use of X-ray Diffraction Peak Broadening Analysis to Characterise Ground Al_2O_3 Powders, *J. Mater. Sci.,* 1985, **20,** p 1266-1274
30. W.C. Oliver and G.M. Pharr, An Improved Technique for Determining Hardness and Elastic Modulus using Load and Displacement Sensing Indentation Experiments, *J. Mat. Res.,* 1992, **7,** p 1564-1580
31. K. Niihara, R. Morena, and D.P.H. Hassleman, Indentation Fracture Toughness of Brittle Materials for Palmquist Cracks, *Fracture Mechanics of Ceramics,* R.C. Bradt, A.G. Evans, D.P. Hassleman, and F.F. Lange, Ed., Plenum Press, 1983, p 97-105
32. K. Niihara, R. Morena, and D.P.H. Hassleman, Evaluation of KIC of Brittle Solids by the Indentation Method with Low Crack to Indent Ratio, *J. Mater. Sci. Lett.,* 1982, **1,** p 13-16
33. H. Chen and C.X. Ding, Nanostructured Zirconia Coatings Prepared by Atmospheric Plasma Spraying, *Surf. Coat. Technol.,* 2002, **150,** p 31-36
34. M. Mohanty, R.W. Smith, M. De Bonte, J.P. Celis, and E. Lugscheider, Sliding Wear Behaviour of Thermally Sprayed 75/25 Cr_3C_2-NiCr Wear Resistant Coatings, *Wear,* 1996, **198,** p 251-266
35. J.M. Guilemany and J.A. Calero, Thermal Spray: Structural Characterisation of Chromium Carbide Nickel Chromium Coatings Obtained by HVOF Spraying. *A United Forum for Scientific and Technological Advances,* C.C. Berndt, Ed., ASM International, 1997, p 15-18
36. R. Morrel, *Properties of Engineering Ceramics, Handbook of Properties of Technical and Engineering Ceramics—Part I,* HMSO, 1989, p 17-208
37. S. Ramalingam, New Coatings Technologies for Tribological Applications, *Wear Control Handbook,* M.B. Peterson and W.O. Winer, Ed., ASME, 1980, p 385-411
38. K. Jia, T.E. Fischer, and B. Gallois, Microstructure, Hardness and Toughness of Nanostructured and Conventional WC-Co Composites. *Nanostruct. Mater.,* 1998, **10,** p 875-891
39. M.M. Lima, C. Goday, P.J. Modenesi, J.C. AvelarBatista, A. Davision, and A. Matthews: Coating Fracture Toughness Determined by Vickers Indentation—An Important Parameters in Cavitation Erosion Resistance of WC-Co Thermally Sprayed Coating, *Surf. Coat. Technology,* 2004, **177-178,** p 489-496
40. Y. Xie and H.M. Hawthorne, The Damage Mechanisms of Several Plasma Sprayed Coatings in Controlled Scratching, *Wear,* 1999, **233-235,** p 293-305